Research Article

Single-Grain Luminescence Dating of Sediment Surrounding a Possible Late Pleistocene Artifact from the Wenas Creek Mammoth Site, Pacific Northwest, USA

Patrick M. Lubinski,[1,*] James Feathers,[2] and Karl Lillquist[3]

[1]Department of Anthropology, Central Washington University, Ellensburg, Washington
[2]Luminescence Dating Laboratory, University of Washington, Seattle, Washington
[3]Department of Geography, Central Washington University, Ellensburg, Washington

Correspondence
*Corresponding author;
E-mail: lubinski@cwu.edu

Received
21 December 2012
Accepted
29 July 2013

Scientific editing by Andreas Lang

Published online in Wiley Online Library (wileyonlinelibrary.com).

doi 10.1002/gea.21461

Excavations at the Wenas Creek Mammoth Site yielded mammoth, bison, and two possible artifacts in a single colluvial stratum, with radiocarbon bone dates ~17 ka. Eight infrared-stimulated luminescence (IRSL) samples were collected to establish general ages of site strata, returning multi-grain estimates consistent with stratigraphic integrity and the radiocarbon dates. Four additional IRSL samples were collected to estimate the depositional age of one artifact found in place. These produced a pooled total of 94 single-grain estimates from near the artifact, 80% averaging 16.8 ± 0.9 ka, and 20% averaging 5.1 ± 0.5 ka. These results could be interpreted to demonstrate pre-Clovis age artifact deposition consistent with the bone dates, or a mid to late Holocene intrusion into older deposits, possibly by bioturbation. The single-grain IRSL dates do not provide proof of pre-Clovis presence beyond reasonable doubt at this site, but do show that this technique is valuable in assessing the stratigraphic integrity needed for any such claim.

INTRODUCTION

At present, the earliest distinctive and well-established archaeological complex in North America dates ca. 11,500 ^{14}C yr BP and is recognized by Clovis artifacts (Anderson & Faught, 2000; Holliday, 2000; Meltzer, 2004; Waters & Stafford, 2007). Many sites with purported human activity dating earlier than 11,500 ^{14}C yr BP are not widely accepted, due to perceived problems with dating, unconvincing evidence of human activity (e.g., artifacts or human remains), association of artifacts and dates, and/or because they are not yet published in sufficient detail for convincing peer review (Haynes, 1969; Dincauze, 1984; Meltzer, 2004). Recently, there have been published claims of pre-Clovis age human activity at several sites in the Pacific Northwest, including Manis at about 11,900 ^{14}C yr BP (Waters et al., 2011), Ayer Pond at 11,990 ^{14}C yr BP (Kenady et al., 2011), and Paisley Caves at about 12,300 ^{14}C yr BP (Gilbert et al., 2008). These claims are being subject to review by the scientific community (e.g., Gilbert et al., 2009; Goldberg, Berna, & Macphail, 2009; Poinar et al. 2009). Another Pacific Northwest site with possible pre-Clovis age human activity is the Wenas Creek Mammoth site (Figure 1).

The Wenas Creek Mammoth site is a find of late Pleistocene mammoth and bison bones from central Washington State (Lubinski et al., 2007). Initial radiocarbon bone dates and bracketing sediment luminescence dates indicated the bones were deposited about 13,000–14,000 ^{14}C yr BP or 15,500–17,000 cal yr BP (Lubinski et al., 2007). In addition to the faunal remains, one possible chipped stone artifact (a flake fragment) of unknown age was found in place ~15 cm above the bones in the same geological stratum (Lubinski et al., 2009). Given the pre-Clovis age of the underlying bones, the age of this specimen is of considerable interest. Here, we describe attempts to determine the depositional age of the artifact by dating single-grains within the sediment that surrounds it, an approach seeing increasing use in assessing the age of possible pre-Clovis artifacts (e.g., Feathers et al., 2010).

The Study Site and Artifact

The study locality is on a laterally discontinuous bench on the south wall of the Wenas Creek Valley (Figure 2). It lies on a footslope ~170 m below the top of the interfluve between Wenas Creek and the Naches River, and

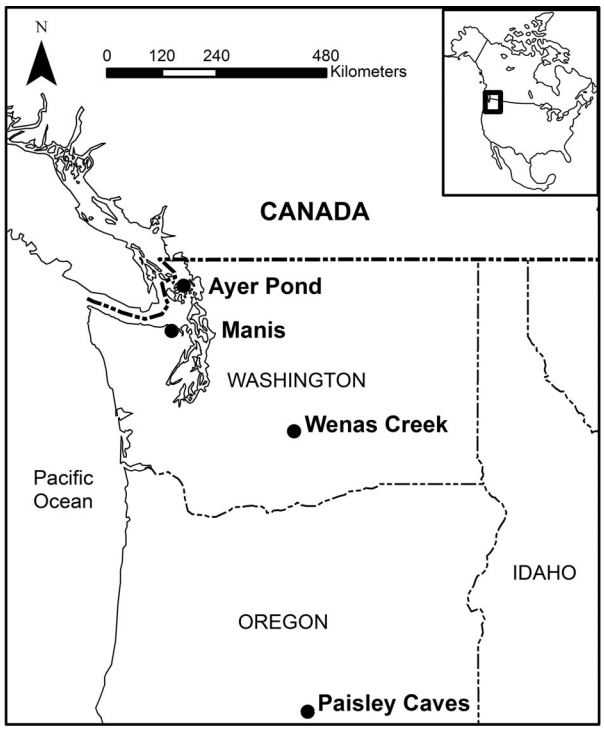

Figure 1 Location of the Wenas Creek site and other sites mentioned in the text.

21 m above the Wenas Creek floodplain. The site locale is shown on the surface geology map (Bentley & Campbell, 1983) as near the center of a ~800 m wide and 400 m long Quaternary mass wasting deposit. This deposit modifies an interfluvial ridge composed of the Tertiary-age Ellensburg Formation, made up primarily of fluvial and lahar-derived fines and gravels in the site vicinity (Bentley & Campbell, 1983). The soil survey (Lenfesty & Reedy, 1985) shows the locality in the Roza clay loam, 15–30% slopes, which is a very deep, well-drained upland soil. The Roza series is an aridisol, specifically a fine, smectic, mesic Xerertic Haplocambid (Natural Resource Conservation Service, 2002).

The find, named the Wenas Creek Mammoth site (45YA1083), was discovered during 2005 construction of a private road across the bench. It was the subject of annual Central Washington University summer investigations from 2005–2010, under the direction of Lubinski. The excavations recovered mammoth (*Mammuthus* sp.) and bison (*Bison* sp.) remains from a ~20–50 cm thick, matrix-supported gravelly silt loam diamicton (Stratum II), interpreted as colluvium. Throughout the excavations, this stratum was overlain by a silty loam ~60–80 cm thick (Stratum I) interpreted as loess, and underlain by more than 180 cm of bedded sands and gravels interpreted as side stream alluvium (Stratum III). These three strata appear to persist at least 50 m up the hillside above the site and 90 m downslope below the site, based on exploratory stratigraphy pits dug off-site. These pits show that Stratum I loess thickens downslope from 48 cm in the uppermost pit to 77 cm in the lowest downslope pit, while Stratum II varies more irregularly from 26 to 59 cm thick. The three strata extended laterally across all excavated units. The likely source for Stratum II is mass wasting of Ellensburg Formation deposits from uphill of the site.

The age of the bones recovered from Stratum II has been estimated with eight bone collagen AMS radiocarbon dates (Table I). When calibrated with the CALIB 6.1.1. radiocarbon calibration program (Stuiver, Reimer, & Reimer, 2012), these eight dates provide a mean pooled age of 13,874 ± 24 ^{14}C yr BP, with individual 2σ ranges from 16,000 to 17,460 cal yr BP (16.0–17.5 ka). Seven of the eight dates have 1σ overlap from 16.9–17.0 ka. These dates indicate the mammoth and bison buried at the site died at about 17 ka.

Two possible artifacts were found in the excavation, but only one in place while the other was found in the screen. Both are described elsewhere (Lubinski et al., 2009) and are the subject of another paper in preparation that will provide detailed information with which to evaluate their validity. In the present paper, the reader is asked to assume the artifacts are in fact made by humans, and consider the question of artifact age.

The single artifact found in situ (FS 261, catalog no. 176) is the focus here. This is a flake fragment (Sullivan & Rosen, 1985) made of red cryptocrystalline silicate and measuring about 13 × 16 × 3 mm. It resembles a lamellar flake or blade fragment, with prominent parallel dorsal arises (Figure 3). The artifact was found within the same stratum and about 15 cm above the nearest bone (Figure 4), an undated mammoth-size metapodial (FS279; catalog no. 198). Although the artifact was not found in direct association with the bones, it could possibly be contemporaneous because it is in the same colluvial stratum with no apparent bedding.

Two preliminary sediment dates provided by the University of Illinois at Chicago (Forman, 2006) bracket the Stratum II-Stratum III contact in the central portion of the excavation. Both dates employed infrared-stimulated luminescence (IRSL) on sediment samples collected by Lubinski. Dating methods followed Forman and Pierson (2002). The sample near Stratum II base (UIC 1688) returned a date of 13.93 ± 1.19 ka, while the sample near Stratum III top (UIC 1203) returned a date of 18.24 ± 1.58 ka. (All IRSL dates in this paper are given as ka or thousands of years before AD 2010). These IRSL dates are consistent at 2 σ with deposition of the mammoth and bison bones near the time of death as estimated by the

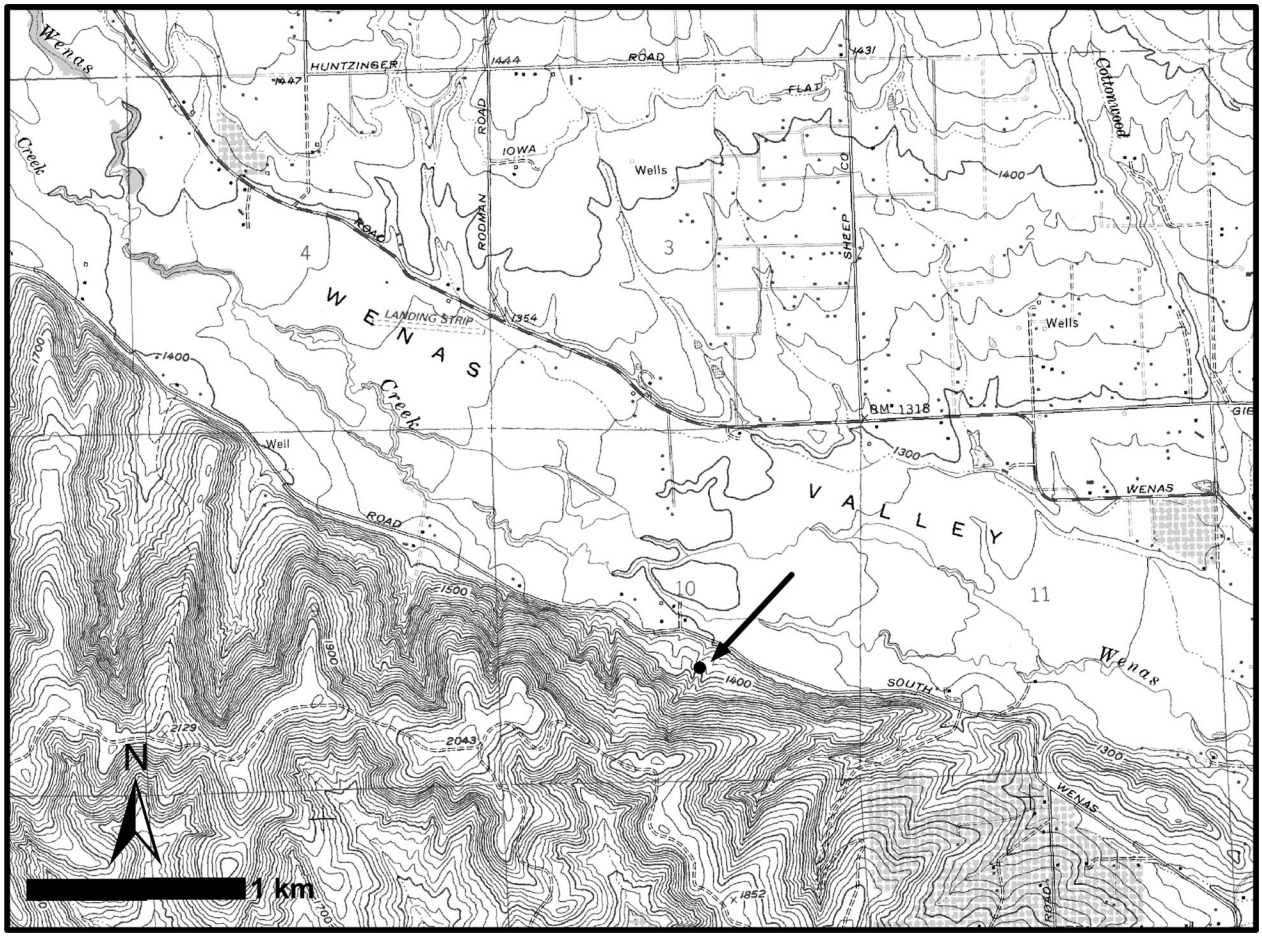

Figure 2 Location of the Wenas Creek site (dot) in relation to the local topography. Base map is from United States Geological Survey (1985).

radiocarbon method. However, the coarse nature of the IRSL age estimates also allow deposition of the bones at the site as late as 11.5 ka, based on the young end of the 2σ range for UIC 1688.

Field evidence suggests stratigraphic integrity and relatively little bioturbation. Krotovina more than 15 mm in diameter were observed rarely, and mostly in Stratum I. In the lower portion of Stratum I, there were numerous small, vertically oriented krotovina interpreted as cicada burrow casts within the B-horizon. Very few krotovina were observed within Stratum II at the site. Additionally, there was a dearth of microfaunal remains recovered from 1/16 in wet screening samples throughout the site. The mammoth and bison remains strongly suggest integrity of at least the lower portion of Stratum II in which they were found. This interpretation is based on the consistent radiocarbon age estimates, the generally good condition of the bones, the lack of significant subaerial weathering except on upper surfaces of a few larger bones, and the presence of some conjoining fragments and anatomical refits across up to 7.7 m of the bonebed.

Framework for Testing

The question of the age of artifacts possibly associated with mammoth bone deposits is hardly unique to the Wenas Creek site. Two recent articles in this journal also address this problem. Pitulko (2011) found that the artifacts at the Berelekh site in Siberia could not be conclusively linked with the Berelekh paleontological bonebed using spatial relationships or radiocarbon dates. Haynes et al. (2013) found that the artifacts at the U.P. Mammoth site in Wyoming are likely but not definitively associated with the mammoth remains spatially and stratigraphically. In both of these cases, the original investigation was many years ago and the precise stratigraphic provenance of many finds is now uncertain. The Wenas Creek site is similar in its uncertain association of artifacts and mammoth bones, but unlike these others in that a suspected

Table I Wenas Creek Mammoth Site AMS radiocarbon dates

Lab number	Material	Raw age (1σ ^{14}C yr BP)	Calibrated age[a] (2σ cal yr BP)
Wk-18064	Mammoth humerus FS1[b]	13,398 ± 58	15,995–16,856
OxA-16755	Mammoth humerus FS1[b]	14,010 ± 90	16,824–17,435
Wk-20117	Bison metatarsal FS275	13,788 ± 70	16,720–17,092
OxA-24804	Bison tibia FS599	14,040 ± 65	16,849–17,438
OxA-24805	Mammoth-size rib FS326	14,035 ± 65	16,845–17,432
OxA-24806	Mammoth-size ulna FS219	14,060 ± 65	16,862–17,458
OxA-24807	Mammoth-size ulna FS219	14,065 ± 65	16,866–17,463
OxA-24808	Mammoth-size ulna FS872	13,770 ± 65	16,712–17,071

[a]Maximum extent of 2σ age ranges calibrated with CALIB 6.1.1 (Stuiver et al. 2012) using intcal09 dataset (Reimer et al. 2009).
[b]Another AMS bone collagen ^{14}C assay from the same mammoth humerus was rejected as anomalously young and internally inconsistent. The sample [Beta-207938] yielded two assays over 1000 years apart at 9730 ± 40 and 11,000 ± 40 ^{14}C yr BP.

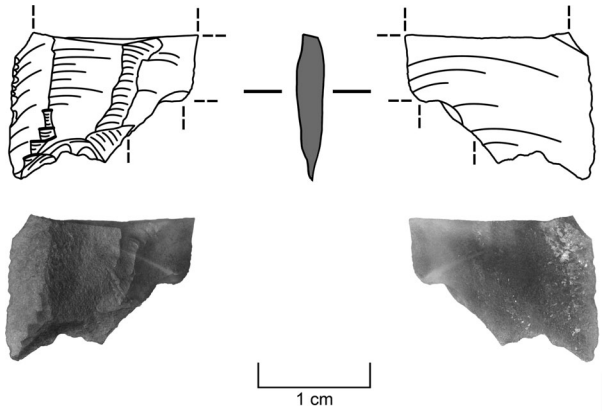

Figure 3 Artifact found in situ (FS 261 and catalog no. 176). Distal end is to top. Pairs of parallel lines indicate areas of fracture.

artifact was unambiguously recorded in the same stratigraphic unit as the mammoth bones.

At the Wenas Creek locality, given that Stratum II is colluvial, this stratum and its constituent bones and artifacts were likely redeposited from a location uphill. There are several possible scenarios for deposition of artifact FS 261. It may have been deposited together with Stratum II and the bones. In this case, the IRSL dates for Stratum II would provide an age for artifact deposition. Alternatively, artifact FS 261 may not have been in close proximity to the bones in the initial deposit, and came to rest close to the mammoth and bison bones only after a mass wasting event. This is especially likely if Stratum II represents multiple mass wasting events, with an earlier event depositing the bones and lower Stratum II, and a later event depositing FS 261 and upper Stratum II. In this case, IRSL dates from around the artifact and in the upper portion of Stratum II would provide a minimum depositional age, which might be notably different and later from the IRSL age of the lower Stratum II sediment and associated radiocarbon dates on bone. A third possibility is that FS 261 was moved into the Stratum II deposit sometime after the bones and most of the Stratum II sediment, such as from bioturbation. In this case, IRSL dates from around the artifact may show a mixture of depositional ages, or a uniform depositional age, depending on the degree or pattern of mixing.

It should be remembered that the age of deposition measured by luminescence dating is a minimum age for artifacts or bones. Artifact production must predate its deposition into the site, although the time lag between these two events is unknown. The bone radiocarbon ages (deaths of mammoth and bison) also must predate their deposition, but given the proclivity of bone for subaerial weathering and lack of extensive weathering of the Wenas Creek bone, it is unlikely there is a significant time lag between these events at the site.

In order to distinguish between the possible scenarios for artifact depositional history and provide an age estimate for the artifact, sediment samples were collected for IRSL dating from as near as possible to the artifact find location in Stratum II. Additional samples taken from elsewhere at the site in all three strata were to allow evaluation of consistency in age estimates for each stratum, establish a chronology for the general site stratigraphy, complement radiocarbon bone dates, and supplement prior sediment dates obtained on Strata II and III from the University of Illinois at Chicago. Single-grain dating was planned for all samples in order to evaluate sediment mixing by comparing of age estimates of multiple individual grains within each sediment sample.

METHODS

Twelve sediment samples for luminescence dating were collected in the field by the authors in August 2008. Samples were taken in three groups: a set of four bracketing the artifact in the adjacent west profile wall, a set of seven spanning the stratigraphy at the south edge of the excavation, and a single sample at the lowest point of the excavation (Table II, Figure 5). The four samples bracketing the artifact were taken from the same stratum, with one

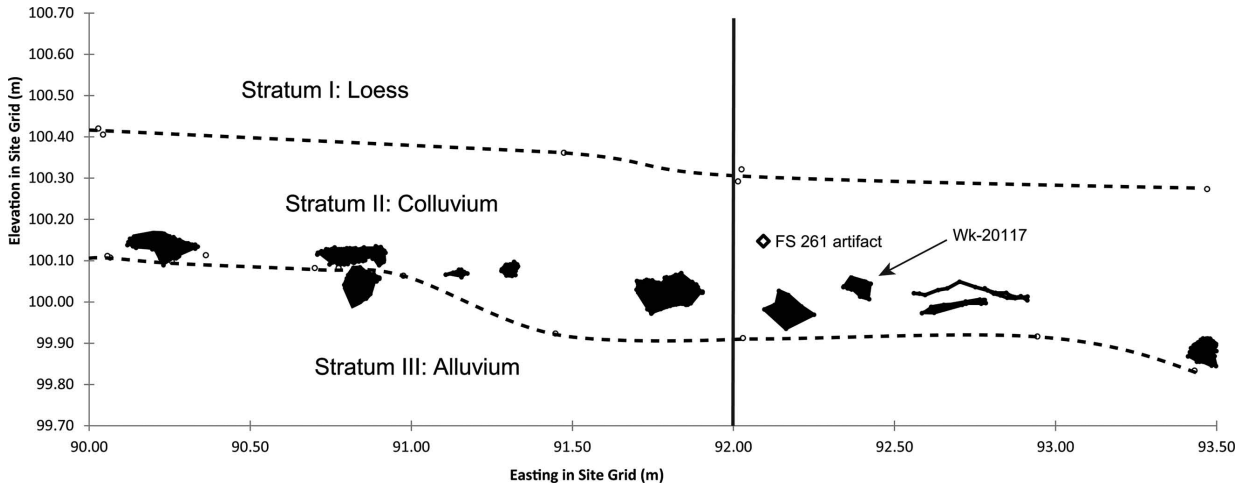

Figure 4 Elevation backplot (modeled East-West cross-section) showing artifact, bones, and strata. Graph shows all total station data for a 30 cm wide strip (500.70–501.00 m North) from 90.0–93.5 m East. Black polygons are all bones mapped within these coordinates. Wk-20117 is a radiocarbon sample (see Table I) from the indicated bone. Open circles are stratum boundary data points. Both stratum boundaries are wavy and gradual (5–15 cm thick) to diffuse (>15 cm). Vertical line is location of profile shown in Figure 6.

Table II Luminescence sediment sample locations

Laboratory #	Field #	Stratum	Unit	Depth (cm below current surface)
UW1887	OSL1	3 (lower)	XU13	152
UW1888	OSL2	3 (top)	XU13	99
UW1889	OSL3	2 (base)	XU13	87
UW1890	OSL4	2 (top)	XU13	69
UW1891	OSL5	1 (base)	XU13	62
UW1892	OSL6	1 (mid, above b-horizon)	XU13	33
UW1893	OSL7	1 (top)	XU13	10
UW1894	OSL8	2 (top, S of flake)	XU12	22[a]
UW1895	OSL9	2 (mid, S of flake)	XU12	35[a]
UW1896	OSL10	2 (base, S of flake)	XU12	56[a]
UW1897	OSL11	2 (mid, N of flake)	XU12	29[a]
UW1898	OSL12	3 (lowest)	XU20	233[a]

[a]Surface was stripped by construction equipment in 2005, so depth before construction was greater.

above, one below, and two stratigraphically equivalent to the artifact (one to either side; see Figure 6).

Samples were collected with opaque cylinders, capped in the field, and returned to the Luminescence Dating Laboratory at the University of Washington for analysis. After removal, copper capsules containing $CaSO_4$:Dy dosimeters were inserted into the removed sample locations and 30–40 cm away from the excavation wall surface. These were left for a year before being retrieved in August 2009. These 12 dosimeters along with a travel dosimeter (which measures any radiation absorbed enroute) were delivered to the laboratory 15 days after retrieval.

The target particles for dating were fine sand-sized (180–212 μm) potassium feldspars, after it was determined that adequate signals could not be obtained from quartz grains because of poor sensitivity. IRSL was used to determine equivalent dose (D_e), which is a measure of the dose absorbed since the last zeroing event and is derived by calibrating the natural signal against signals induced by laboratory irradiation. Dividing D_e (in Gy, the SI unit of absorbed dose) by the time-averaged natural dose rate (Gy per unit time) produced each age estimate.

To determine the dose rate, sample radioactivity was first measured in the lab by alpha counting in conjunction with atomic emission for ^{40}K. Samples for alpha counting were crushed in a mill to flour consistency, packed into plexiglass containers with ZnS:Ag screens, and sealed for one month before counting. The pairs technique was used to separate the U and Th decay series. For atomic emission measurements, samples were dissolved in HF and other acids and analyzed by a Jenway flame photometer. K concentrations for each sample were determined by bracketing between standards of known concentration. Conversion to ^{40}K was by natural atomic abundance. Radioactivity was also measured, as a check, by beta counting, using a Risø low-level beta GM multicounter system. About 0.5 g of crushed sample was placed on each of four plastic sample holders. All were counted for 24 hours. The average was converted to beta dose rate following Bøtter-Jensen and Mejdahl (1988) and compared with the beta dose rate calculated from the alpha counting and flame photometer results. After the $CaSO_4$ dosimeters were returned to the laboratory, their luminescence signal was measured by

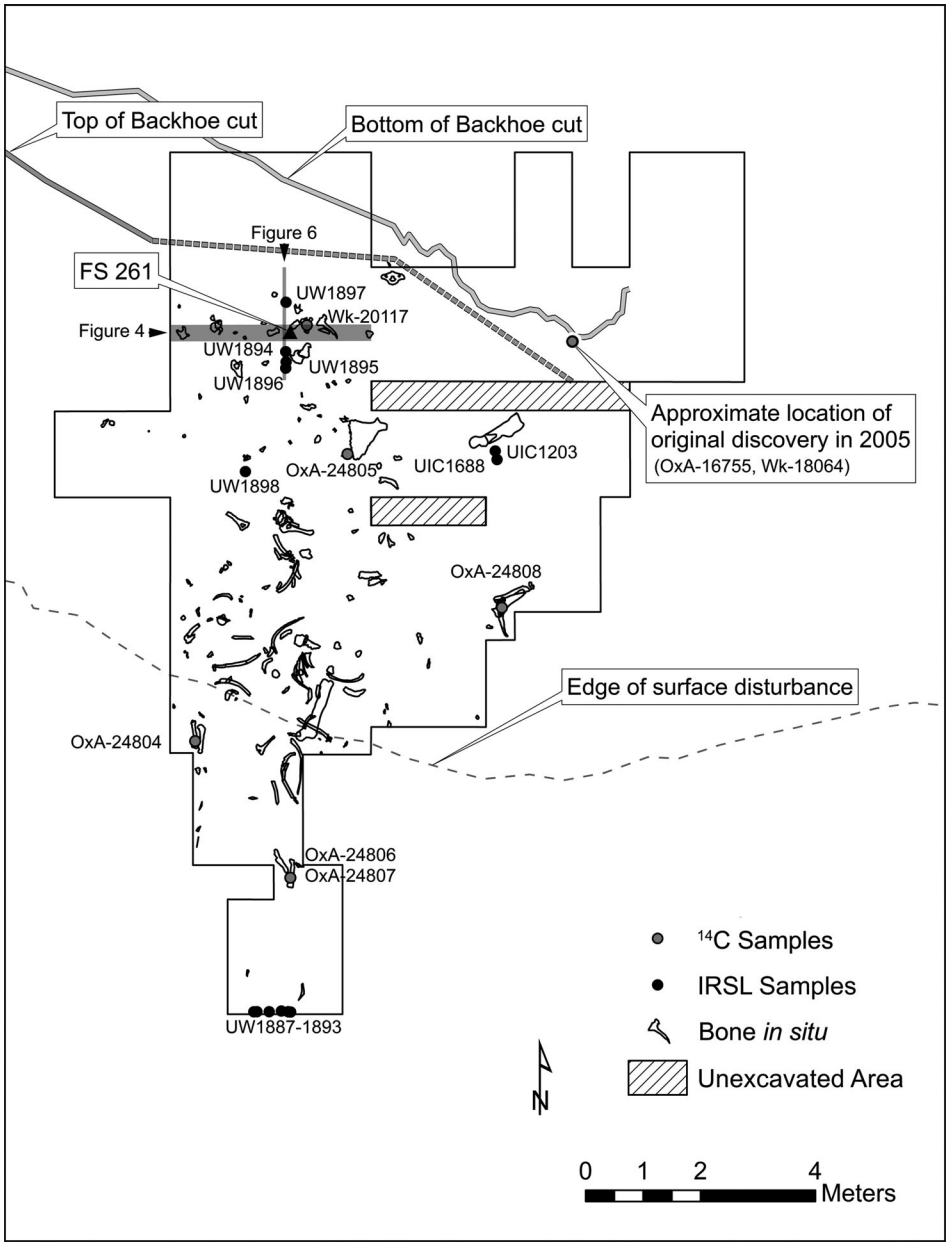

Figure 5 Plan view of locations of dating samples compared to artifact and bone. Note the positions of Figure 4 (a backplot East-West through the location of the FS261 artifact), and Figure 6 (a profile North-South through the location of the artifact and its IRSL samples) indicated with gray.

thermoluminescence and calibrated against a beta source. The source was used with the shutter closed to provide a low calibrating dose, about 0.001 Gy/1000s. Cosmic radiation was determined after Prescott and Hutton (1988). Radioactivity concentrations were translated into dose rates following Adamiec and Aitken (1998).

To determine equivalent dose, unexposed portions of each sample were first wet-sieved through a 90 μm screen. The >90 μm fraction was treated with HCl and H_2O_2, and then dry-sieved to isolate the 180–212 μm fraction. A portion of four samples was etched with 48% HF for 40 min and density separated using a solution of lithium metatungstate set at 2.67 specific gravity. The quartz obtained by this procedure produced no measurable ultra-violet luminescence signals when excited by green or blue light. No further work was done with quartz. Instead, sample preparation focused on feldspars. Non-etched 180–212 μm grains were density separated using lithium metatungstate set at 2.58 specific gravity. Luminescence measurements were made on the

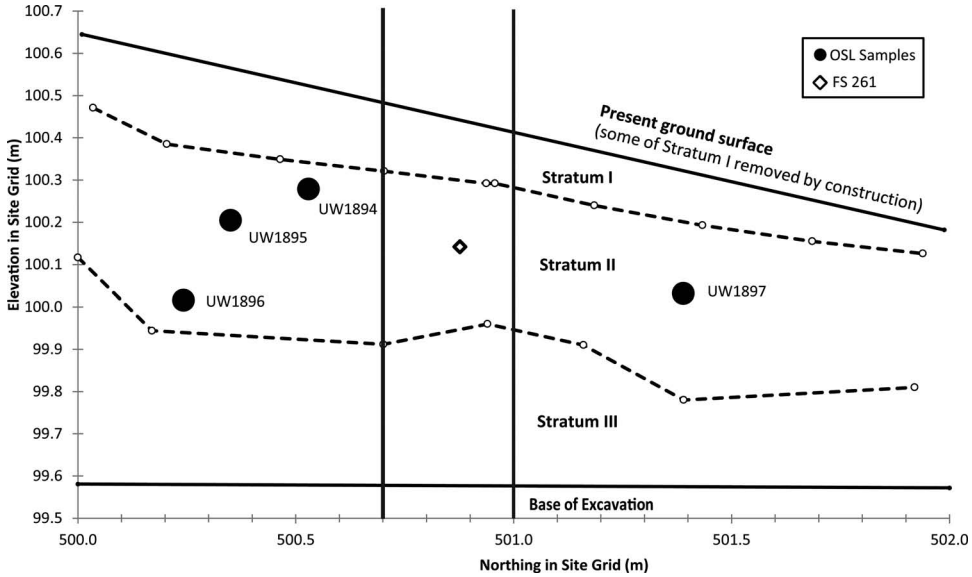

Figure 6 Location of artifact (FS 261) and dating samples on the adjacent west profile wall (500–502 m North and 92 m East). Open circles are stratum boundary data points. Both stratum boundaries are wavy and gradual (5–15 cm thick) to diffuse (>15 cm). Vertical lines indicate extent of elevation backplot shown in Figure 4.

<2.58 fraction. With feldspars, correction for anomalous fading, which is athermal loss of trapped charge through time, is required.

Single-grain dating was attempted for all samples, although due to insensitivity of the grains, it was applied comprehensively only to the four samples surrounding the artifact. Both single-grain and multi-grain single aliquot measurements were made using either a Risø TL/OSL DA-15 or TL/OSL DA-20 reader, the latter with an IR single-grain attachment. Stimulation for single-grains used a 150 mW 830 nm IR laser, set at 90% power and passed through an RG 780 filter. It was realized later that such intensity produced considerable heat during measurement, sometimes sufficient to shatter the grains, although it is not certain if this had any significant effect on results. Stimulation for multi-grain aliquots used an LED array emitting at 875 nm at 135 mW/cm^2 (again at 90% power). Emission was collected by the photomultiplier through a blue-filter pack, allowing transmission in the 350–450 nm range. IRSL measurements were made at 50°C, and a preheat of 250°C for 1 minute at 5°C/s preceded each measurement. Exposure for single-grains was for 0.8 s, using the first 0.06 s for analysis and the last 0.15 s for background. Exposure for multi-grain aliquots was for 95 s, using the first 5 seconds for analysis and the last 15 seconds for background.

Equivalent dose (De) was determined using the single-aliquot regenerative dose (SAR) protocol (Murray & Wintle 2000; Wintle & Murray 2006), and as applied to feldspars by Auclair et al. (2003). The SAR method measures the natural signal and the signal from a series of regeneration doses on a single aliquot. The method uses a small test dose to monitor and correct for sensitivity changes brought about by preheating, irradiation, or light stimulation. The SAR and fading correction protocol is given in Table III. A zero regeneration dose and a

Table III SAR and fading correction protocol for single grains/aliquots

1. Dose (either natural or applied)
2. Heat 250°C for 1 min
3. IRSL (830nm) 1s, 50°C (Lx)
4. Test dose ~ 6 Gy
5. Heat 250°C for 1 min
6. IRSL (830nm) 1s, 50°C (Tx)
7. Repeat steps 1–6 using following doses after the natural: 24, 12, 36, 48, 60, 0, 24 Gy
8. Determine De by interpolating Ln/Tn into growth curve constructed with Lx/Tx values
9. Dose of 12 Gy
10. Heat 250°C for 1 min
11. Store for different lengths of time up to 5 days
12. IRSL (830 nm) 1s, 50°C (Fx)
13. Test dose ~ 6 Gy
14. Heat 250°C for 1 min
15. IRSL (830 nm) 1s, 50°C (Tx)
16. Repeat steps 9–15 for 15 times using different storage times, every other one being a prompt delay of just the irradiation and preheat
17. Determine *g*-value from slope of linear fit to Fx/Tx values plotted against log storage time

repeated regeneration dose are employed to insure the procedure is working properly.

Test doses for the SAR were about 5–6 Gy. Doses were delivered by a ^{90}Sr beta source, which provides about 0.10 or 0.12 Gy/s to 180–212 μm grains, depending on the machine used. The beta sources were calibrated at both single- and multi-grain levels using quartz irradiated by a gamma source at Battelle Laboratory in Hanford, Washington. The dose delivered to different grains in single-grain disks varied by an order of magnitude from one end of the disk to the other. This variation was taken into account when determining doses to individual grains.

An advantage of single-grain dating is the opportunity to remove from analysis grains with unsuitable characteristics by establishing a set of criteria grains must meet. Grains are eliminated from analysis if they (1) had poor signals (as judged from net natural signals not at least three times above the background standard deviation), (2) did not produce, within 20 percent, the same signal ratio (often called recycle ratio) from identical regeneration doses given at the beginning and end of the SAR sequence, suggesting inaccurate sensitivity correction, (3) yielded natural signals that did not intersect saturating growth curves, (4) had a signal larger than 10 percent of the natural signal after a zero dose, or (5) produced a zero D_e (within 1-sigma of zero).

A dose recovery test was performed on some single- and multi-grain aliquots. The luminescence was first removed by exposure to the laser or LEDs (using the same parameters mentioned earlier). A dose of known magnitude was then administered. The SAR procedure was then applied to see if the known dose could be obtained. Successful recovery was an indication that the procedures were appropriate.

Anomalous fading was measured using the procedures of Auclair, Lamothe, and Huot (2003) for both multi-grain aliquots and single grains (see Table III). Seven delay times, ranging up to 3–5 days, were employed for every aliquot, without moving the aliquot or grain. Several "prompt" delays (only considering the time of irradiation and preheat) were also employed. Age was corrected following Huntley and Lamothe (2001).

A fading-corrected age was obtained for each suitable grain or aliquot. Because of varying precision and other factors, the same value is not obtained for each grain or aliquot even if all are of the same true age. Instead a distribution is produced. The common age model and central age model of Galbraith (Galbraith & Roberts, 2012) are statistical tools that were used in evaluation of age distributions. The common age model controls for differential precision by computing a weighted average using log values. The central age model is similar except rather than assuming a single true value it assumes a natural distribution of estimated age values, even for true single-aged samples, because of nonstatistical sources of variation that are not accounted for in the estimations, such as variation of luminescence properties among grains or heterogeneity in dose rate. It computes an overdispersion parameter (σ_b) interpreted as the relative standard deviation (or coefficient of variance) of the true age estimates, or, in other words, that deviation beyond what can be accounted for by measurement error. Empirical evidence suggests that σ_b of between 10 and 20 percent for single-grains and 2–5 percent for multi-grain aliquots are typical for single-aged samples (Olley, Pietsch, & Roberts, 2004; Jacobs, Duller, & Wintle, 2006). Overdispersion will be higher for samples that are not single-aged because of partial bleaching or postdepositional mixing.

For the single-grain age distributions, a finite mixture model was also employed for evaluation. This model (Galbraith & Roberts, 2012), which is appropriate for samples where postdepositional processes have mixed grains of different depositional age, uses maximum likelihood to separate the grains into single-aged components based on the input of a given σ_b value and the assumption of a log normal distribution of each component. The model estimates the number of components, the weighted average of each component, and the proportion of grains assigned to each component. The model provides two statistics for estimating the most likely number of components, maximum log likelihood and Bayes Information Criterion. The finite mixture model is most useful for samples that have discrete rather than continuous age populations due to mixing.

RESULTS

Dose Rate

Table IV gives for each sample the concentration of the major radionuclides as determined on bulk samples from alpha counting and flame photometry, and the beta dose rate calculated in the two ways described earlier. Note that alpha counting was not completed for UW1896. U and Th values for this sample were estimated using beta counting and assuming secular equilibrium. The difference in beta dose rates between the two methods is not significant for any sample. That and the general similarity among all samples in radioactive composition suggest no significant dose rate changes through time or deviation from secular equilibrium, at least from the top of the U decay chain. If there is radon escape, it is assumed to be constant through time and reflected in the alpha counting, which measures actual alpha dose rates. Measured moisture content is also given in Table IV. A value of

Table IV Radionuclides, beta dose rate, and moisture content of samples

Sample	^{238}U (ppm)	^{232}Th (ppm)	K (%)	Beta dose rate (Gy/ka)[b]		Measured moisture (%)
				ß-counting	α-counting/flame photometry	
				0.96 ± 0.10	0.98 ± 0.05	7.7
UW1888	1.09 ± 0.08	1.24 ± 0.43	0.98 ± 0.04	0.99 ± 0.09	0.96 ± 0.03	4.9
UW1889	0.96 ± 0.10	5.25 ± 0.81	1.01 ± 0.07	1.15 ± 0.13	1.08 ± 0.06	4.3
UW1890	0.87 ± 0.08	2.99 ± 0.67	1.02 ± 0.06	1.05 ± 0.13	1.00 ± 0.05	4.4
UW1891	1.00 ± 0.11	5.33 ± 0.90	1.08 ± 0.03	1.10 ± 0.09	1.13 ± 0.04	4.4
UW1892	1.07 ± 0.08	1.84 ± 0.49	0.99 ± 0.14	1.07 ± 0.10	0.98 ± 0.11	3.8
UW1893	0.93 ± 0.08	2.45 ± 0.60	1.01 ± 0.06	1.07 ± 0.09	0.99 ± 0.05	1.9
UW1894	0.30 ± 0.09	6.32 ± 0.98	0.96 ± 0.05	0.97 ± 0.05	1.01 ± 0.08	5.9
UW1895	1.04 ± 0.09	2.56 ± 0.62	0.90 ± 0.03	1.03 ± 0.09	0.92 ± 0.03	4.9
UW1896	1.20 ± 0.10	3.85 ± 0.70	0.95±0.04	1.02 ± 0.10	1.02 ± 0.10[a]	6.0
UW1897	1.11 ± 0.10	3.89 ± 0.69	0.95 ± 0.09	1.03 ± 0.09	1.01 ± 0.08	6.2
UW1898	0.61 ± 0.07	3.02 ± 0.67	0.95 ± 0.08	0.93 ± 0.08	0.92 ± 0.06	5.8

[a]U and Th values were adjusted to make beta dose rate equal to that from beta counting for this sample only (UW1896). This is because the beta dose rate calculated from alpha counting (assuming equilibrium) and flame photometry did not agree with that from beta counting. We assumed the results from beta counting, as a direct measure, were more reliable.
[b]Uncorrected for moisture content.

5 ± 5% was used for most samples, based on measured values. For UW1887 and UW1893 (at the bottom and top of the southern excavation wall), respective values of 8 ± 5 and 2 ± 3% were used. The climate has been dry through most of the samples' history (Whitlock et al., 2000; Blinnikov, Busacca, & Whitlock, 2002).

Table V gives the measured external dose rate from the dosimeters and that calculated from the laboratory measurements, as well as the total dose rate calculated either using the dosimeter measurements or using the laboratory measurements. There is a significant difference in the total dose rate for only three samples. The external dose rate from the dosimeter and from the lab measurements were averaged (weighting by precision) for all samples, except for these three, and the total dose rate using the average (also given in Table V) was used for age

Table V Moisture-corrected dose rates of samples

Sample	Internal dose rate (Gy/ka)		External dose rate (Gy/ka)			Total dose rate (Gy/ka)		
				Gamma + Cosmic[b]				
	Alpha	Beta[a]	Gamma	Dosimeter	Laboratory	With dosimeter	All laboratory	Weighted average
UW1887	0.06 ± 0.04	0.93 ± 0.08	0.48 ± 0.04	0.58 ± 0.13	0.66 ± 0.06	1.65 ± 0.11	1.57 ± 0.16	1.64 ± 0.10
UW1888	0.04 ± 0.02	0.95 ± 0.08	0.44 ± 0.03	0.52 ± 0.12	0.63 ± 0.05	1.62 ± 0.10	1.51 ± 0.14	1.60 ± 0.09
UW1889	0.07 ± 0.04	1.03 ± 0.09	0.55 ± 0.05	1.15 ± 0.11	0.74 ± 0.06	1.86 ± 0.12	2.26 ± 0.15	
UW1890	0.05 ± 0.03	0.98 ± 0.09	0.46 ± 0.04	1.06 ± 0.08	0.68 ± 0.06	1.71 ± 0.11	2.09 ± 0.12	
UW1891	0.07 ± 0.05	1.08 ± 0.08	0.54 ± 0.04	1.00 ± 0.21	0.75 ± 0.06	1.91 ± 0.11	2.16 ± 0.23	1.93 ± 0.11
UW1892	0.05 ± 0.03	0.97 ± .013	0.43 ± 0.05	0.83 ± 0.09	0.67 ± 0.07	1.69 ± 0.15	1.84 ± 0.16	1.74 ± 0.15
UW1893	0.05 ± 0.03	1.00 ± 0.08	0.40 ± 0.03	0.69 ± 0.15	0.68 ± 0.07	1.74 ± 0.11	1.74 ± 0.17	1.74 ± 0.10
UW1894	0.06 ± 0.04	0.94 ± 0.08	0.54 ± 0.05	0.77 ± 0.11	0.76 ± 0.07	1.76 ± 0.12	1.77 ± 0.15	1.76 ± 0.11
UW1895	0.05 ± 0.03	0.91 ± 0.08	0.43 ± 0.04	0.83 ± 0.07	0.64 ± 0.06	1.61 ± 0.10	1.79 ± 0.11	1.68 ± 0.09
UW1896	0.05 ± 0.03	0.99 ± 0.08	0.52 ± 0.04	0.88 ± 0.09	0.73 ± 0.06	1.77 ± 0.11	1.92 ± 0.13	1.82 ± 0.10
UW1897	0.06 ± 0.04	0.98 ± 0.10	0.51 ± 0.05	0.84 ± 0.07	0.73 ± 0.07	1.77 ± 0.13	1.89 ± 0.13	1.82 ± 0.12
UW1898	0.04 ± 0.03	0.90 ± 0.09	0.42 ± 0.04	1.38 ± 0.20	0.58 ± 0.05	1.52 ± 0.11	2.19 ± 0.14	
UW1894–1897								1.76 ± 0.05

[a]The beta dose rate includes an internal dose of 0.12 ± 0.04 Gy/ka for all samples. The beta dose rate also differs from that given in Table IV because of correction for moisture content.
[b]Cosmic dose rate varies from 0.16 to 0.28, depending on burial depth. For specific samples it can be obtained by subtracting the gamma dose rate from the laboratory gamma plus cosmic dose rate.

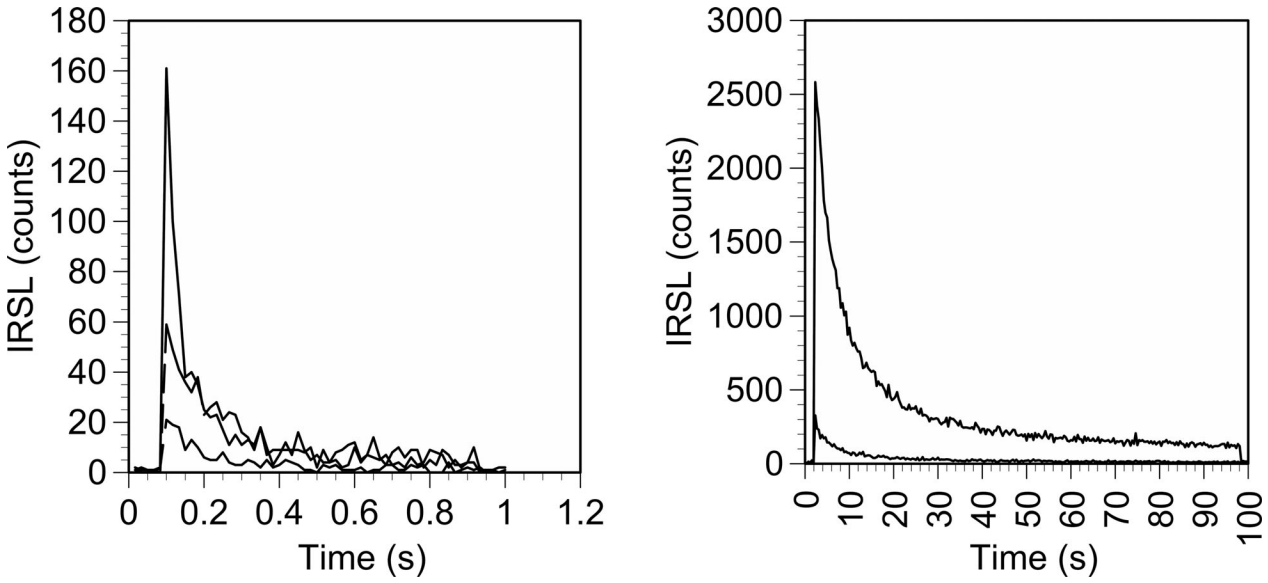

Figure 7 IRSL decay curves for three single grains from UW1894 (left) and two multi-grain aliquots from UW1894 and UW1890 (right). The first few points represent machine background before the laser or diodes are turned on. The peak represents the first point after the laser or diodes are turned on.

calculation. The dose rates for the four samples located around the artifact were averaged for age calculations for those samples, because the D_e values were combined for these samples. For the three where the dosimeter and lab measurements differed, age was calculated in both ways. Stratigraphy was used to judge which gave the more consistent age.

The total dose rates also reflect an internal dose rate from K-feldspar grains. K content was determined by x-ray energy dispersive analysis (EDS) on individual grains using a scanning electron microscope (SEM). Single-grains used for D_e measurement of UW1894 were removed with tape from the single-grain disks and affixed to an SEM sample stub retaining the grid configuration so that EDS measurements could be taken on the same grains used for D_e. Because of time and financial constraints, only 36 grains could be measured, 18 that produced a measurable IRSL signal and 18 that did not. It was discovered that the grains could not be classified as K-feldspars (despite using the 2.58 specific gravity density solution), as they averaged only $2.0 \pm 0.8\%$ K content by weight, compared to 14% expected for pure orthoclase. No significant difference in K-composition was detected for grains that did (2.0%) or did not (2.1%) have an IRSL signal. Average Na and Ca contents for grains with signal were 4.0% and 2.6%, respectively. The grains appeared to be mixtures of different kinds of feldspars. An EDS analysis of all 100 grains from one disk yielded a K content of $2.4 \pm 0.8\%$ and this was used for estimating the internal K for all samples. It is not expected that variation in internal K will have any significant effect in the dispersion of D_e values among grains.

Equivalent Dose

D_e was determined from 6–18 multi-grain aliquots per sample. Of the 120 total aliquots measured, none were rejected because of the criteria listed earlier. A total of 7965 single grains were measured. Of these, only 160 were accepted, a rate of only 2%. Most of the rejections were due to a signal not measurable above background. The other criteria mentioned above accounted for only 81 rejections, about 1%. Recycle failures and zero doses accounted for 61 of these. Of the 160 accepted, another 28 were rejected because the fading correction yielded infinite ages due to very high measured fading rates. That left 132 grains for which an age could be determined. Due to the low acceptance rate, it was decided to concentrate the single-grain analysis on the four samples surrounding the flake (UW1894–7), which produced 94 of the single-grain ages. Sample decay curves and luminescence with dose growth curves are shown in Figures 7 and 8.

The distribution of D_e values within a single sample, whether multi-grain or single-grain aliquots, is not meaningful because of differential fading rates from aliquot to aliquot. Therefore distribution analysis will only concern the corrected ages, to be discussed in the next section.

It is, however, useful to evaluate the appropriateness of the procedures followed. This was done with the dose recovery test. A total of 779 grains, about 200 each from

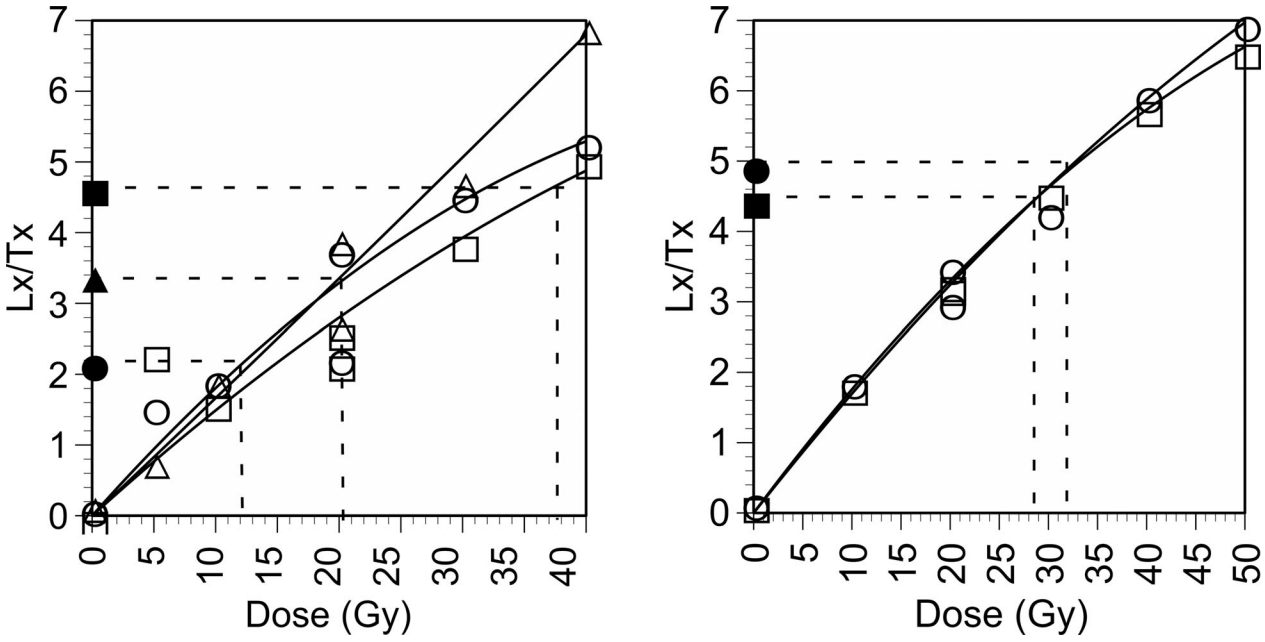

Figure 8 Curves showing growth of luminescence with dose for the same single grains and multi-grain aliquots depicted in the previous figure. The solid symbols represent the natural signal. The open symbols represent the regeneration doses. The y-axis is Lx/Tx as explained in Table III. The horizontal dotted lines are the interpolation of the natural doses into the growth curves. The vertical dotted lines show the dose at which the interpolation occurs, or the equivalent dose. Fits are saturating exponentials. Error bars are left out for ease of illustration.

the four samples surrounding the flake (UW2294–7), were measured, using an administered dose of 200 s of beta irradiation. Twenty-two grains produced a measurable signal, using the criteria mentioned earlier. Two of these produced anomalously low values, but the other 20 produced a weighted average D_e (from the central age model) of 201 ± 11 s of beta, nearly identical to the administered dose, with an overdispersion of 10.4%. Including the two low values gives an average of 190 ± 19 s of beta with overdispersion of 35.6%, still within error terms of the administered dose but with much higher scatter. Discounting the two low outliers, 60% of the grains produced a D_e within 1σ of the administered dose, and 95% were within 2σ. These results suggest the procedures are appropriate, although the two outliers remain unexplained. The 10% overdispersion indicates that scatter of at least that magnitude should be expected in a natural sample even if all grains are the same age. For multi-grain single aliquots, only 1 disk from each of the four samples was measured for dose recovery. The weighted average result is 209 ± 9 s of beta with no overdispersion.

Fading rates were highly variable. For multi-grain aliquots, the range in g-value (% fading per decade, where a decade is a power of 10, and normalized to 2 days) is from 0 to 11%. Taking out two negative values, the weighted average ($n = 118$) is 4.9 ± 0.2%, with overdispersion of 27%. For single-grains, the range is from several negative values to over 50. To account for differential precision, the negative values ($n = 55$) were changed to zero (on the assumption they were not statistically different from zero, since it is impossible to have negative fading) and the weighted average became 10.0 ± 1.0%, with overdispersion of 59%, but weighted average biases against low values. The median value, for example, is only 3%. Precision in g-value was much more variable for the single-grains than the single aliquots. Figure 9 plots the luminescence signal against log storage time to show the fading rates. Note the difference in scatter between the two single-grains and between them and the single aliquot.

Figure 10 plots the equivalent dose against g-value for both single-grains and single-aliquots for the four samples from around the flake. The solid line is a linear fit to the data. Even though scatter is high, in part because of differential precision, both plots show g-value decreasing with higher equivalent dose. This is what would be expected for single-aged samples and also shows that fading is highly variable from grain to grain. Equivalent dose will vary with the fading rate, making any distribution of equivalent dose values rather meaningless by themselves.

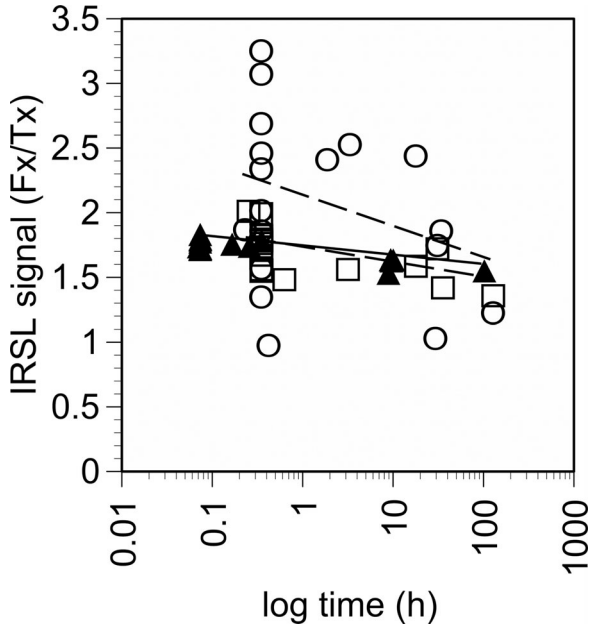

Figure 9 Anomalous fading as shown as loss of signal with log time for two single-grains (open circles and open squares) and one multi-grain aliquot (closed triangles). Although error bars are not included for ease of illustration, they are much larger for the single-grains than the multi-grain aliquots. Note the low scatter for the multi-grain aliquot, relatively low scatter for one of the single grains (squares) but very high scatter for the other one (circles). Dotted lines are log linear fits. The units on the Y-axis are explained in Table III.

Age Estimates

Table VI gives the sample ages using the central age model (and using ages corrected for anomalous fading) and the overdispersion for each sample. In the tabulations, two outlying values were removed: a multi-grain aliquot from UW1889, which gave an age of about 135 ± 40 ka, and a single-grain from UW1888, which gave an age of 4.5 ± 1.2 ka. Neither value comes anywhere close to reflecting the age of the deposit or to values from other aliquots/grains in those two samples. They remain unexplained. In evaluating sample size, remember that each multi-grain aliquot contains about 1000 grains, the luminescence signals for which are averaged. The central age given in Table VI for the multi-grain aliquots is thus in a sense an average of averages, while for single-grains it is an average of single-values.

The multi-grain and single-grain central ages agree for all samples but four, and in these four the single-grain sample size is relatively small. For the four samples around the flake (UW1894–7), where the single-grain sample size is relatively large, there is no significant difference. This suggests that nothing in either the single-grain or the multi-grain procedures (such as the high heat from the single-grain laser or averaging from the multi-grain analysis) is creating significant bias. Secondly, consideration of stratigraphy allows evaluation of the different dose rates (dosimeter vs. laboratory) detected for three of the samples, as discussed earlier. The higher

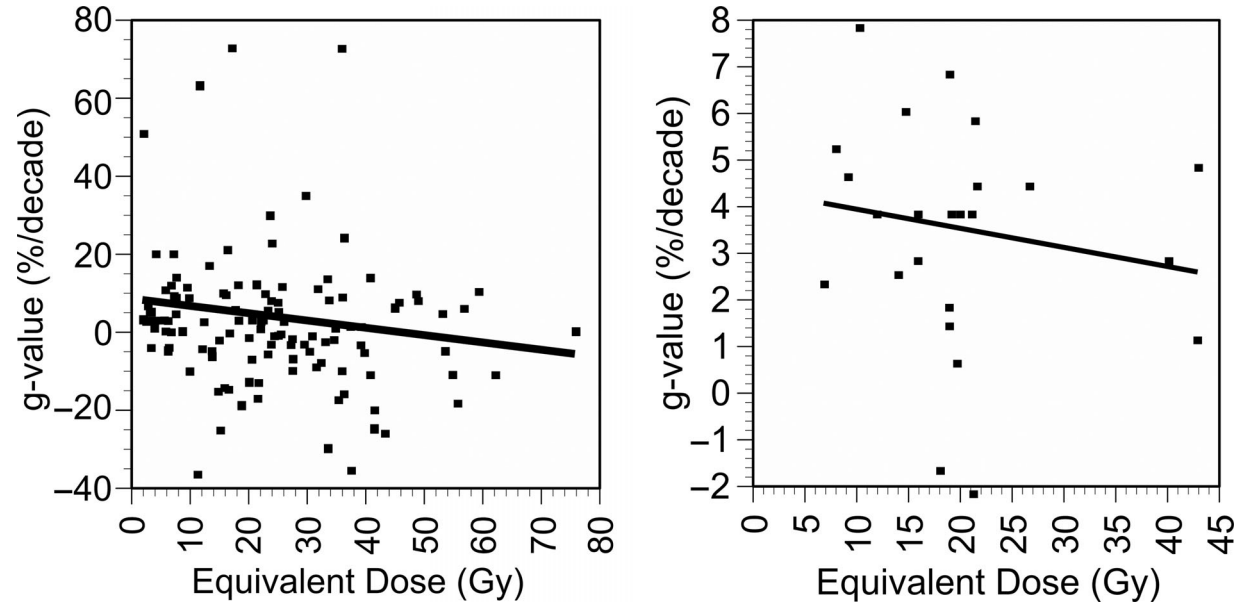

Figure 10 Plot of equivalent dose versus *g*-values for single-grains (left) and multi-grains (right), both for samples UW1894-UW1897, which should all be about the same age. The solid lines are linear fits to the data. Although there is much scatter, owing largely to errors in *g*-value (the errors are not shown for clarity), *g*-value decreases with increasing equivalent dose, which is what would be expected for a single-aged sample.

Table VI IRSL age estimates. For three samples (UW1889, 1890, 1898), the dose rate (DR) measured in the laboratory and the rate measured with the dosimeters varied, and both rates and resulting ages are provided here. All other samples had agreement between dose rates from the laboratory and dosimeter

Sample	Analysis[a]	N	Central age (ka)	σ_b (%)
UW1887	MG	12	25.0 ± 1.6	14.4
	SG	5	28.0 ± 12.5	82.6
UW1888	MG	12	28.0 ± 4.5	45.1
	SG	6	24.0 ± 4.4	13.1
UW1889 DR = 2.3 (Gy/ka)	MG	17	20.2 ± 1.3	12.8
	SG	1	22.3 ± 3.1	
UW1889 DR = 1.9 (Gy/ka)	MG	17	24.6 ± 1.6	12.5
	SG	1	27.1 ± 3.7	
UW1890 DR = 2.1 (Gy/ka)	MG	18	20.1 ± 1.8	34.2
	SG	6	15.0 ± 1.4	0
UW1890 DR = 1.7 (Gy/ka)	MG	18	24.8 ± 2.3	34.2
	SG	6	18.4 ± 1.8	0
UW1891	MG	18	20.7 ± 1.1	15.6
	SG	4	14.2 ± 1.4	0
UW1892	MG	6	9.2 ± 0.8	13.2
	SG	1	46.7 ± 54.5	
UW1893	MG	6	8.0 ± 2.5	74.5
	SG	11	15.1 ± 2.8	49.1
UW1894	MG	6	14.2 ± 1.8	21.2
	SG	33	16.9 ± 2.3	51.9
UW1895	MG	6	8.2 ± 1.1	24.9
	SG	29	9.2 ± 1.6	72.0
UW1896	MG	6	18.4 ± 3.4	32.9
	SG	12	19.4 ± 3.8	37.7
UW1897	MG	6	16.1 ± 2.1	0
	SG	20	14.9 ± 2.0	29.8
UW1898 DR = 2.9(Gy/ka)	MG	6	19.6 ± 2.2	0
	SG	3	13.1 ± 4.0	0
UW1898 DR = 1.5(Gy/ka)	MG	6	28.4 ± 3.3	0
	SG	3	19.1 ± 6.0	0

[a]SG, single grain aliquots; MG, multi-grain single aliquots.

dose rate from laboratory measurements for UW1889 and UW1890 produce ages closer in agreement to UW1894–7, which come from the same stratum, suggesting the dosimeter readings are not accurate for these samples. On the contrary, the dose rate using the dosimeter for UW1898 makes the age for this sample consistent with the stratigraphy, while the higher laboratory dose rate puts the sample out of stratigraphic order.

Overdispersion values vary considerably both for single-grain and multi-grain aliquots. This will be discussed first for the four samples around the flake: UW1893–7, which generally have much higher overdispersion than would be expected from the dose recovery data if they were single-age samples, from either multi-grain or single-grain aliquots. It is not likely that differential beta dose rate is a principal cause of the high overdispersion. Internal K is low and not very variable among grains, and no other source of differential dose rate—such as uneven distribution of low radioactive inclusions such as carbonates—is readily apparent, except perhaps from bones. But none of the samples were close enough to any bones to affect the beta distribution.

The four samples from around the artifact all came from the same stratum and are relatively close to each other, but the central age value for UW1895 is significantly lower than the other samples for both single and multi-grains. The single-grain overdispersion value for UW1895 is also very high, 72%. To investigate we applied the finite mixture model. Using an assumed overdispersion of 10% for a single-aged sample, three of the four samples are statistically consistent with a single age. Only UW1895 divided into two components of about equal size, one with an age of 5.0 ± 0.5 ka and the other with an age of 16.9 ± 2.3 ka. The latter is in agreement with the central age of the other three samples. The sample sizes of all four samples are relatively small, and the

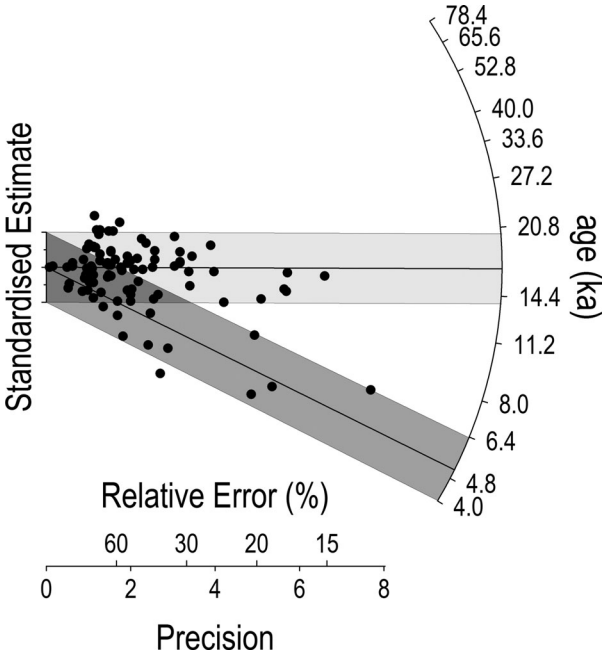

Figure 11 Radial graph of IRSL age distribution for UW1894–1897 samples around flake, corrected for anomalous fading. The shaded region denotes the boundaries of values falling within two standard errors of the mean age.

single-component result of the three samples could be a function of sample size. All four samples from around the flake were thus combined to give a sample size of 94. The finite mixture model was applied to the combined data, again using an assumed overdispersion of 10% for single-aged samples. Two components were resolved (Figure 11), one giving an age of 5.1 ± 0.5 ka and the other an age of 16.8 ± 0.9, almost identical results as that from UW1895 alone. Twenty percent of the ages (about 19 grains) could be assigned to the younger component, more than 2/3 of them (13 grains) coming from UW1895. In sum, there are two sets of grains in these samples, one set which gives an age of around 16.8 ka and that dominates the distributions of three of the samples but comprises only about half (53%) of the distribution from UW1895, and another set that gives an age of around 5 ka and is present mainly in UW1895. We interpret the younger set of ages to represent an intrusion of younger grains, mainly into the area from which UW1895 was drawn. The source of this intrusion is not known but it could be an animal burrow that intersected the sampling area. UW1895 is the middle sample of three collected about 0.5 m south of the flake (see Figure 6). The fact that the older grains in these samples are consistent with a single age argues that neither partial bleaching nor postdepositional mixing is a problem for the other three samples around the flake.

Finite mixture analysis is not appropriate for multi-grain aliquots, because they are averaged data. However, when combining the multi-grain aliquot values for UW1894, UW1896, and UW1897—all arguably samples of the same age—the equivalent dose is 16.0 ± 1.4 (similar to the single-grain age) with an overdispersion of 24.3%. This suggests that overdispersion values that are high for other samples are also single-aged. Such relatively high overdispersion for multi-grain single aliquots for single-aged samples should not be surprising given the low sensitivity of these grains (thus weakening any averaging effects). Only UW1888, UW1890, and UW1893 have multi-grain overdispersion values higher than this.

The high overdispersion for UW1888 is caused by just one aliquot with a young age. The sample is at the top of the same stratum containing UW1887. The central-age ages are statistically identical for both samples. While some intrusion of younger grains in the stratum seems likely, it does not appear significant. The high overdispersion for UW1890 is caused by three younger aliquots. Again this sample is near the top of the stratum in which it is located, and the central age is statistically identical with that from UW1889, which is lower down in the stratum and that has much lower overdispersion. UW1893 is located near the current surface at the top of Stratum 1. It is highly mixed, probably due to current surface processes, e.g., soil development on top of the much older loess.

DISCUSSION AND CONCLUSIONS

The age of artifact FS 261 is best estimated by comparison to the four IRSL samples and one ^{14}C sample taken in close proximity, and more broadly by comparison to IRSL and ^{14}C samples elsewhere in Stratum II. The IRSL and ^{14}C samples taken from within 63 cm of the artifact in Stratum II are in good agreement with the exception of UW1895 as noted above (Table VII, Figure 12). When the 94 single-grain estimates from the four IRSL samples around the artifact are pooled, 80% of them resolve to 16.8 ± 0.9 ka. This age range overlaps with a calibrated 1σ range of 16.4–17.2 ka for all eight radiocarbon dates obtained from bones near the base of Stratum II at the site. The Stratum II IRSL estimates from elsewhere on the site are not quite so closely aligned, although all overlap between 16 and 17.6 ka at 2σ (Figure 13). These other estimates are all from multi-grain aliquots, and averaging could mask some localized mixing. Additionally, the Chicago IRSL dates from Stratum II (UIC 1688) and Stratum III (UIC 1203) may appear younger than the UW dates because they were not corrected for anomalous fading as were the UW samples. Overall, taking into account

Table VII Single-grain age estimates for the artifact-bearing deposit

Sample	*N* (grains)	Position[a]	1σ Age (ka)	2σ Range (ka)
UW 1894	33	Above ~8cm and 35 cm south	16.9 ± 2.3	21.5–12.3
UW1895	29	Same and 52 cm south	9.2 ± 1.6	12.4–6.0
UW1896	12	Below ~20 cm and 63 cm south	19.4 ± 3.8	27.0–11.8
UW1897	20	Same and 52 cm north	14.9 ± 2.0	18.9–10.9
Pooled sample component 1	19	All	5.1 ± 0.5	6.1–4.1
Pooled sample component 2	75	All	16.8 ± 0.9	18.6–15.0

[a]Stratigraphic position of sample center point within Stratum II, followed by lateral position, both relative to artifact.

IRSL ages from all strata, there are no stratigraphic inversions that might indicate wide scale mixing.

Regarding the age of artifact FS261, two different interpretations could be offered. The most liberal interpretation would place the artifact-bearing deposit at 18.6–15 ka, corresponding with the majority of single grain IRSL dates near the artifact and all radiocarbon dates, and accept that most of Stratum II (including the artifact location) is undisturbed. This would mean that the artifact was deposited at about the same time as the bones at the site, and predates Clovis times. This interpretation is supported by the prevalence of 15 ka or older age estimates for the Stratum II deposit, and the lack of evidence for bioturbation. About 80% (75/94) of the single grain samples near the artifact resolved to the older component, with only about 20% dating to the younger component and these mainly from one sample. The lack of significant bioturbation is indicated by the lack of observed krotovina in the artifact-bearing unit profile wall, and is supported by the rarity of krotovina in Stratum II elsewhere at the site, and the dearth of microfauna recovered from 1/8 in wet screening samples at the site.

A more conservative interpretation would accept that most of Stratum II was deposited by 15 ka or earlier, but would argue that the artifact is a later intrusion, possibly as a result of bioturbation. The possibility of postdepositional intrusions that left no obvious krotovina cannot be discounted, as this is the most likely explanation for the 5.0 ± 0.5 ka age estimate for nearly half the grains of IRSL sample UW1895 located 52 cm north of the artifact. In this case, the artifact could be a mid to late-Holocene intrusion into the Pleistocene bone-bearing deposit.

The age of the artifact thus comes down to probability. Most of the single-grain IRSL data suggests stratigraphic integrity of the deposit, including the two samples closest to the artifact, although the closest, UW1894, is still

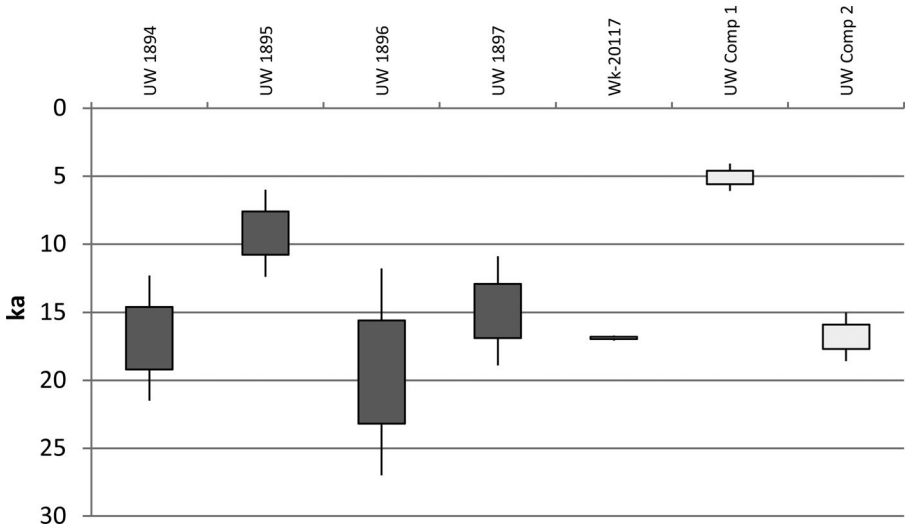

Figure 12 Box and whisker plot of age estimates from around the artifact. Boxes indicate 1σ age ranges and whiskers indicate 2σ age ranges. The white boxes to the right indicate components resolved from the four single grain IRSL dates to the left. IRSL ages are provided as thousands of years before AD 2010(see Table VII). Wk-20117 is a calibrated radiocarbon date, provided as thousands of calendar years before AD 1950 (see Table I), and adjusted to AD 2010 for this graph.

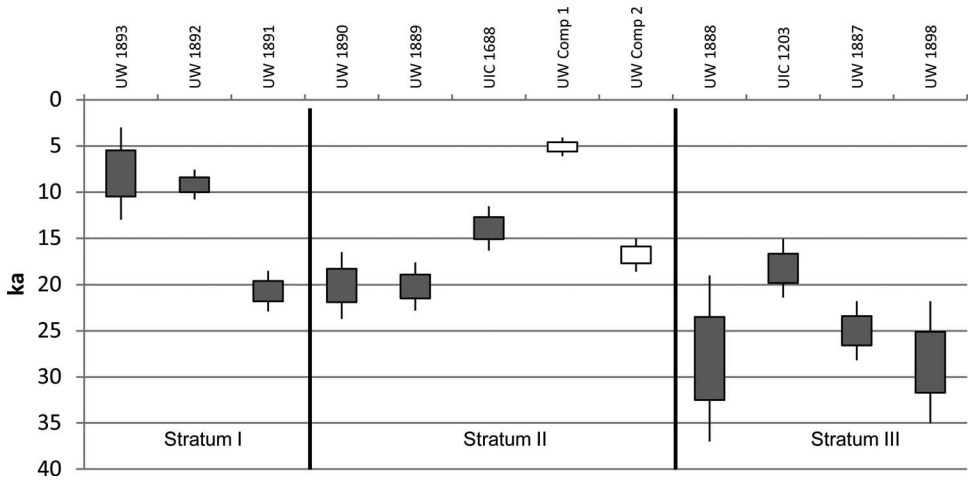

Figure 13 Box and whisker plot of all site IRSL age estimates. Boxes indicate 1σ age ranges and whiskers indicate 2σ age ranges. The white boxes indicate components resolved from the four single grain IRSL dates (UW1894–1897). All other dates are multigrain. All dates except the two components are displayed from top to bottom of stratum from left to right. Ages are provided as thousands of years before AD 2010 (see Table VI).

35 cm south and 13 cm higher in elevation. (Closer samples were not taken, in an attempt to preserve the integrity of the profile.) Thus a pre-Clovis age for the artifact is probable, although the IRSL single-grain analysis also showed that some localized mixing has occurred, in particular for a sample only 52 cm away. Therefore, we cannot discount that some localized mixing may also have occurred at the flake location. Establishment of a pre-Clovis presence in Washington State requires proof beyond reasonable doubt, and that cannot be provided here. We have shown, however, that single-grain luminescence dating is a valuable tool in assessing stratigraphic integrity necessary for any pre-Clovis claim.

The Wenas Creek Mammoth Project has received generous contributions and support from landowners Doug and Bronwyn Mayo, Central Washington University (Faculty Research Fund, Wayne Quirk, Office of Continuing Education, Office of Graduate Studies and Research), field school and laboratory students and volunteers, and private donors. Nate Morse and Karisa Terry produced Figure 3, and Holly Eagleston completed Figure 5. Ian Buvit, Pat McCutcheon, Karisa Terry, and two anonymous reviewers provided helpful comments on the manuscript.

REFERENCES

Adamiec, G., & Aitken, M. J. (1998). Dose rate conversion factors: Update. Ancient TL 16, 37–50.

Anderson, D., & Faught, M. (2000). Paleoindian artifact distribution: Evidence and implications. Antiquity 74, 507–513.

Auclair, M., Lamothe, M., & Huot, S. (2003). Measurement of anomalous fading for feldspar IRSL using SAR. Radiation Measurements 37, 487–492.

Bentley, R.D., & Campbell, N.P. (1983). Geologic map of the Yakima quadrangle, Washington (1:62,500). Geologic Map GM-29. Olympia: Washington State Department of Natural Resources. Available online at: http://www.dnr.wa.gov/publications/ger_gm29_geol_map_yakima_62k.pdf.

Blinnikov, M., Busacca, A., & Whitlock, C. (2002). Reconstruction of the late Pleistocene grassland of the Columbia Basin, Washington, USA, based on phytolith records in loess. Palaeogeography, Palaeoclimatology, Palaeoecology, 177, 77–101.

Bøtter-Jensen, L, & Mejdahl, V. (1988). Assessment of beta dose-rate using a GM multi-counter system. Nuclear Tracks and Radiation Measurements, 14, 187–191.

Dincauze, D. F. (1984). An archaeo-logical evaluation of the case for pre-Clovis occupations. Advances in World Archaeology, 3, 275–323.

Feathers, J. K., Piló, L., Arroyo-Kalin, M., Kipnes, R., & Coblenz, D. (2010). How old is Luzia? Luminescence dating and stratigraphic integrity at Lapa Vermelha, Lagoa Santa, Brazil. Geoarchaeology, 25, 395–436.

Forman, S.L. (2006). Infrared stimulated luminescence (IRSL) ages on the fine-grained polymineral fraction from sediments from a paleontological/archaeological excavation near Selah, Yakima County, Washington. Chicago: University of Illinois at Chicago Luminescence Dating Research Laboratory.

Forman, S. L., & Pierson, J. (2002). Late Pleistocene luminescence chronology of loess deposition in the Missouri and Mississippi river valleys, United States. Palaeogeography, Palaeoclimatology, Paleoecology, 186, 25–46.

Galbraith, R. F., & Roberts, R. G. (2012). Statistical aspects of equivalent dose and error calculation and display in OSL

dating: an overview and some recommendations. Quaternary Geochronology, 11, 1–27.

Gilbert, M.T.P., Jenkins, D.L., Götherstrom, A., Naveran, N., Sanchez, J.J., Hofreiter, M., Thomsen, P.F., Binladen, J., Higham, T.F.G., Yohe, R.M., II, Parr, R., Scott Cummings, L., & Willerslev, E. (2008). DNA from Pre-Clovis human coprolites in Oregon, North America. Science, 320, 786–789.

Gilbert, M.T.P., Jenkins, D.L., Higham, T.F.G., Rasmussen, M., Malmström, M., Svensson, E.M., Sanchez, J.J., Scott Cummings, L., Yohe, R.M. II, Hofreiter, M., Götherström, A., & Willerslev, E. (2009). Response to comment by Poinar et al. on "DNA from Pre-Clovis human coprolites in Oregon, North America." Science, 325, 148-b.

Goldberg, P., Berna, F., & Macphail, R.I. (2009). Comment on "DNA from pre-Clovis human coprolites in Oregon, North America." Science, 325, 148-c.

Haynes, C.V. (1969). The earliest Americans. Science, 166, 709–715.

Haynes, C.V., Surovell, T.A. & Hodgins, G.W.L. (2013). The U.P. Mammoth site, Carbon County, Wyoming, USA: More questions than answers. Geoarchaeology, 28, 99–111.

Holliday, V.T. (2000). The evolution of Paleoindian geochronology and typology on the Great Plains. Geoarchaeology, 15, 227–290.

Huntley, D.J., & Lamothe, M. (2001). Ubiquity of anomalous fading in K-feldspars, and measurement and correction for it in optical dating. Canadian Journal of Earth Sciences, 38, 1093–1106.

Jacobs, Z., Duller, G.A.T., & Wintle, A.G. (2006). Interpretation of single grain D_e distributions and calculation of D_e. Radiation Measurements, 41, 264–277.

Kenedy, S.M., Wilson, M.C., Schalk, R.F., & Mierendorf, R.R. (2011). Late Pleistocene butchered *Bison antiquus* from Ayer Pond, Orcas Island, Pacific Northwest: Age confirmation and taphonomy. Quaternary International 233, 130–141.

Lenfesty, C.D., & Reedy, T.E. (1985). Soil survey of Yakima county area, Washington. Washington, D.C.: Soil Conservation Service.

Lubinski, P.M., Barton, B.R., Lillquist, K., Uebelacker, M., & Shapley, J.T. (2007). The Late-Glacial Wenas Creek mammoth site (45YA1083) in Central Washington. Current Research in the Pleistocene, 24, 178–180.

Lubinski, P.M, McCutcheon, P.T., Lillquist, K., Uebelacker, M., Barton, B.R., & Shapley, J.T. (2009). Possible lithic artifacts from 2005–2007 excavations at the Wenas Creek mammoth site. Current Research in the Pleistocene, 26, 85–86.

Meltzer, D.J. (2004). Peopling of North America. In A.R. Gillespie, S.C. Porter & B.F. Atwater (Eds.), The Quaternary period in the United States (pp. 539–563). Amsterdam: Elsevier.

Murray, A.S., & Wintle, A.G. (2000). Luminescence dating of quartz using an improved single-aliquot regenerative-dose protocol. Radiation Measurements, 32, 57–73.

Natural Resource Conservation Service (2002). Roza Series. Available at: https://soilseries.sc.egov.usda.gov/OSD_Docs/R/ROZA.html (accessed May 21, 2013).

Olley, J.M., Pietsch, T., & Roberts, R.G. (2004). Optical dating of Holocene sediments from a variety of geomorphic settings using single grains of quartz. Geomorphology, 60, 337–358.

Pitulko, V.V. (2011). The Berelekh quest: A review of forty years of research in the mammoth graveyard in northeast Siberia. Geoarchaeology, 26, 5–32.

Poinar, H., Fiedel, S., King, C.E., Devault, A.M., Bos, K., Kuch, M., & Debruyne, R. (2009). Comment on "DNA from pre-Clovis human coprolites in Oregon, North America." Science, 325, 148-a.

Prescott, J.R., & Hutton, J.T. (1988). Cosmic ray and gamma ray dose dosimetry for TL and ESR. Nuclear Tracks and Radiation Measurements, 14, 223–235.

Reimer, P.J., Baillie, M.G.L., Bard, E., Bayliss, A., Beck, J.W., Blackwell, P.G., Bronk Ramsey, C., Buck, C.E., Burr, G.S., Edwards, R.L., Friedrich, M., Grootes, P.M., Guilderson, T.P., Hajdas, I., Heaton, T.J., Hogg, A.G., Hughen, K.A., Kaiser, K.F., Kromer, B., McCormac, F.G., Manning, S.W., Reimer, R.W., Richards, D.A., Southon, J.R., Talamo, S., Turney, C.S.M., van der Plicht, J., & Weyhenmeyer, C.E. (2009). Intcal09 and Marine09 radiocarbon age calibration curves, 0–50,000 years Cal BP. Radiocarbon, 51, 1111–1150.

Stuiver, M., Reimer, P.J., & Reimer, R. (2012). CALIB radiocarbon calibration, PC version 6.1.1. Available at: http://calib.qub.ac.uk/calib/ (verified 4 July, 2012).

Sullivan, A.P. III, & Rosen, K.C. (1985). Debitage analysis and archaeological interpretation. American Antiquity, 50, 755–779.

United States Geological Survey. (1985). 7.5′ topographic quadrangle map for Selah, Washington. Reston, Virginia: United States Geological Survey.

Waters, M.R., & Stafford, T.W., Jr. (2007). Redefining the age of Clovis: Implications for the peopling of the Americas. Science, 315, 1122–1126.

Waters, M.R., Stafford, T.W., Jr., McDonald, H.G., Gustafson, C., Rasmussen, M., Cappellini, E., Olsen, J.V., Szklarczyk, D., Jensen, L.J., Gilbert, M.T.P., & Willerslev, E. (2011). Pre-Clovis mastodon hunting 13,800 years ago at the Manis site, Washington. Science, 334, 351–353.

Whitlock, C., Sarna-Wojcicki, A.M., Bartlein, P.J., & Nickmann, R.J. (2000). Environmental history and tephrostratigraphy at Carp Lake, southwestern Columbia Basin, Washington, USA. Palaeogeography, Palaeoclimatology, Palaeoecology, 155, 7–29.

Wintle, A.G., & Murray, A.S. (2006). A review of quartz optically stimulated luminescence characteristics and their relevance in single-aliquot regeneration dating protocols. Radiation Measurements, 41, 369–391.

